Efficient ethylene purification by a robust ethane-trapping porous organic cage

Kongzhao Su
Fujian Institute of Research on the Structure of Matter
Wenjing Wang
Fujian Institute of Research on the Structure of Matter, Chinese Academy of Sciences
Shunfu Du
Fujian Institute of Research on the Structure of Matter, Chinese Academy of Sciences
Chunqing Ji
Fujian Institute of Research on the Structure of Matter
Daqiang Yuan (ydq@fjirsm.ac.cn)
Fujian Institute of Research on the Structure of Matter https://orcid.org/0000-0003-4627-072X

Article

Keywords: ethylene, porous organic cage, hydrocarbons

Posted Date: November 4th, 2020

DOI: https://doi.org/10.21203/rs.3.rs-98247/v1

Abstract

The removal of ethane (C_2H_6) from its analogous ethylene (C_2H_4) is of paramount importance in the petrochemical industry, but highly challenging due to their similar physicochemical properties. It is still remaining unexploited to utilize emerging porous organic cage (POC) materials for C_2H_4/C_2H_6 separation. Herein, we report the benchmark example of a truncated octahedral calix[4]resorcinarene-based POC adsorbent (**CPOC-301**), preferring to adsorb C_2H_6 than C_2H_4, and thus can be used as a robust absorbent to directly separate high-purity C_2H_4 from the C_2H_4/C_2H_6 mixture. Molecular modelling studies suggest the exceptional C_2H_6 selectivity is due to the suitable resorcin[4]arene cavities in **CPOC-301**, which form more multiple C–H···π hydrogen bonds with C_2H_6 than with C_2H_4 guests. This work provides a fresh avenue to utilize POC materials for highly selective separation of industrially important hydrocarbons.

Introduction

Ethylene (C_2H_4), the largest feedstock in petrochemical industries with a global production capacity of more than 170 million tons in 2018, exceeds any other chemical feedstock molecules for its wide application in the manufacture of polyethylene[1]. The industrial separation of C_2H_4 from ethane (C_2H_6) is typically by cryogenic distillation at high pressure and very low temperature condition, with very high towers, because they have similar sizes and volatilities[2]. Such process is extremely energy consuming, and thus exploration of other effective C_2H_4 separation methods at ambient condition are highly demanded. Selective adsorption by porous materials to produce high-purity C_2H_4 has been determined to be one of the most desired methods for its low energy consumption[3,4]. Of particular recent interest in this region is the use of C_2H_6-selective porous materials enriched with nonpolar/inert surfaces (e.g., featuring aromatic or aliphatic moieties), because they prefer to capture more polarizable C_2H_6, and thus can directly produce high purity C_2H_4 in a single adsorption step, avoiding an additional high-energy-consuming desorption step[5,6]. So far, most of the developed C_2H_6-selective adsorbents are metal – containing materials[6–10]. However, the polar metal centers in these materials can interact with unsaturated C_2H_4 molecules via strong π-complexation interactions, and thus reduce their C_2H_4/C_2H_6 separation abilities[11]. Thus, it is very necessary to develop other C_2H_6-selective adsorbents such as metal-free organic porous materials[12,13], because they cannot only avoid the abovementioned problem, but also are easier to construct inert surface. However, the research of such materials is still in the initial stage[14].

Porous organic cages (POCs), as a new type of porous materials, are intrinsically porous given their hollow cavities[15–20]. The discrete inherent nature of the POCs makes them possessing distinct advantages in solution processing, regeneration and post-synthesis modification[20–23]. Since the first elegant work reported in 2009 by Cooper et al.[24], the number of POCs with different shapes, sizes and

properties has increased substantially[25–35], but robust POCs with high surface areas are still few, which highly hinder their practical applications in gas storage and separation. In the past decade, although the Brunauer-Emmett-Teller (BET) surface areas of the POCs have increased from the initial 624 $m^2 g^{-1}$ to 3758 $m^2 g^{-1}$, the majority of POCs have BET values less than 1000 m^2/g[36,37]. As for gas separation, Cooper and coworkers first reported that imine-linked tetrahedral POC (**CC3**) exhibits unprecedented selectivity of 20.4 for rare gas Xe/Kr separations at low rare gas concentrations in 2014[38]. Two years later, they showed that **CC3** could also separate sulfur hexafluoride (SF_6), a much more potent greenhouse gas than carbon dioxide, from nitrogen (N_2) with the highest SF_6/N_2 selectivity reported for any material at ambient condition[39]. The selectivity for the abovementioned two cases is arising from the precise size match between the Xe and SF_6 with the organic cage cavity than Kr and N_2, respectively. In 2019, their team utilized post modification synthesis method to modify the internal cavities of **CC3** to produce hybrid cocrystal material (**6ET-RCC3-R**/**CC3-S**), which are excellent quantum sieves for hydrogen isotope separation with excellent deuterium/hydrogen selectivity (8.0)[40]. In the same year, Zhang's and Zaworotko's groups presented a soft imide-based POC (**NKPOC-1**) with gate opening behavior and can highly efficiently separate binary or ternary C3 hydrocarbon mixtures[41]. Up to now, POC adsorbents have only been limited to the above gas separations, and thus there is still much room to explore new POC materials for gas separations applications, especially for industrially important gases.

Calix[4]resorcinarenes, a subset of calixarenes, were derived from the acid-catalyzed condensation of resorcinol with various kinds of aldehydes[42–44]. They possess electron-rich π cavities and eight upper-rim phenolic groups, and have been determined to be effective hosts for inclusion of a variety of guests range from small gases to large organic molecules[44–48]. Notably, their upper rims can be easily functionalized, and this makes them good molecular building blocks for construction of self-assembled cages as well as porous polymers[49–55]. Very recently, by using pre-designed concave-shaped tetraformylresorcin[4]arene (RC4ACHO) as secondary building blocks and different diamine as linkers, our group have systematically designed and synthesized several porous POCs with structural diversity from [2 + 4] dimeric lanterns, [3 + 6] trimeric triangular prisms, to [6 + 12] hexameric octahedra[56]. However, utilization of calix[4]resorcinarene-based POCs as solid adsorbents for gas separation applications is still unexploited. Herein, we present that the robust and highly porous [6 + 12] octahedral calix[4]resorcinarene-based POC (**CPOC-301**) is an excellent C_2H_6-selective material, and can be used as a robust absorbent to directly produce high-purity C_2H_4 from C_2H_4/C_2H_6 mixture.

Results

Crystal structure and characterization of CPOC-301

As shown in Fig. 1a, **CPOC-301** was successfully prepared via self-assembly of RC4ACHO (1 equiv.) and p-phenylenediamine (2 equiv.) under mild condition. Single-crystal X-ray diffraction reveals that **CPOC-301** has a truncated octahedron structure, with eight trigonal ports with an edge length of about 12 Å, and

a large cavity with inner diameter and volume of 16.8 Å and 4270 $Å^3$, respectively. The solid-state packing of **CPOC-301** suggests that it possesses a one-dimensional channel, with a diameter of ~ 7 Å, viewed from the [001] direction (Fig. 1b). Notably, the quantitative tautomerization of the imines in **CPOC-301** to their keto-enamine forms has been observed from ^{1}H NMR and FT-IR spectroscopy (Supplementary Figs. 1–3). Such a transformation makes **CPOC-301** more stable even when it is stored in air for over half a year, as has been confirmed by FT-IR spectra as well as ^{1}H NMR studies (Supplementary Figs. 3 and 4). TGA suggests that **CPOC-301** is thermally stable up to 300 ^oC under an N_2 atmosphere (Supplementary Fig. 5). PXRD reveals that the desolvated **CPOC-301** retains its crystal packing (Supplementary Fig. 6), which is very uncommon in large POC systems.

Gas adsorption and separation performances

The channel-type structure of **CPOC-301** can potentially lead to interesting solid-state gas sorption properties. The permanent porosity of the activated **CPOC-301** was confirmed by N_2 gas sorption experiments at 77 K (Fig. 2). Its N_2 adsorption isotherm shows a typical type I curve with a small fraction of a type II adsorption behavior. The maximum N_2 adsorption is 670 $cm^3\ g^{-1}$, and the calculated BET of **CPOC-301** is up to 1962 $m^2\ g^{-1}$. The pore volume and the micropore volume of **CPOC-301** are 1.03 $cm^3\ g^{-1}$ and 0.46 $cm^3\ g^{-1}$, respectively. The PSD profile exhibits a relatively sharp distribution of micropores from 1.59 nm to 1.77 nm (Fig. 2 inset), which accords well with the cavity size of **CPOC-301** in the crystal structure.

The high surface area and high density of nonpolar calix[4]resorcinarene cavities in **CPOC-301**, which may favor the preferential adsorption of more polarizable C_2H_6 in preference to C_2H_4, prompted us to investigate the sorption of these gases. Single-component adsorption isotherms of **CPOC-301** for C_2H_6 and C_2H_4 were measured at 273 K, 283 K and 293 K at 1 bar. Notably, **CPOC-301** exhibits preferential adsorption of C_2H_6 (87 $cm^3\ g^{-1}$) to C_2H_4 (75 $cm^3\ g^{-1}$) at 293 K (Fig. 3a), and also the other two temperatures (Supplementary Figs. 7 and 8). The corresponding isosteric heat of adsorption (Q_{st}) at zero coverage for C_2H_6 and C_2H_4 was calculated to be 32.4 and 24.2 kJ mol^{-1}, respectively (Fig. 3b and Supplementary Figs. 9 and 10). Such a difference suggests that the host-guest interactions between **CPOC-301** and C_2H_6 are much stronger than that of C_2H_4. Notably, the C_2H_6 uptake capacity of **CPOC-301** at 293 K and 1 bar exceeds that of all the reported porous organic materials[14], and most of the reported C_2H_6-selective MOF materials[5].

Motivated by the high uptake capacity and C_2H_6-selective behavior of **CPOC-301**, the ideal adsorbed solution theory (IAST) is used to evaluate the separation selectivity of C_2H_4/C_2H_6 (50:50) (Supplementary Figs. 11–13). IAST calculation results show that the C_2H_6/C_2H_4 selectivity range is from 1.3 to 1.4 at 293 K. To evaluate the actual separation performance of **CPOC-301**, the experimental breakthrough studies were conducted in a packed column of the activated **CPOC-301** sample under an equimolar C_2H_4/C_2H_6 mixture at ambient conditions. The breakthrough curves shown in Fig. 3c prove that **CPOC-**

301 can efficiently realize the complete separation of C_2H_4 from C_2H_4/C_2H_6 mixtures. Notably, the C_2H_4 gas breaks through the adsorption bed first to yield an outflow of pure gas containing no detectable C_2H_6. Conversely, the C_2H_6 gas breaks through the column following a substantial time-lapse, because the C_2H_6 molecule is more preferentially adsorbed in **CPOC-301** than C_2H_4. From the dynamic breakthrough experiment, the separation factor was calculated to be 1.3 for an equimolar mixture of C_2H_4/C_2H_6, which is consistent with the predicted IAST result. For practical industrial applications, the ideal adsorbent should also have good recycling performance. We performed multiple C_2H_4/C_2H_6 mixed-gas dynamic breakthrough experiments under similar operating conditions. The separation performance of C_2H_4/C_2H_6 does not obviously change within seven continuous cycles (Fig. 3d), and the NMR and PXRD data after breakthrough experiments (Supplementary Figs. 14 and 15), indicate that **CPOC-301** is robust enough to be a promising candidate for C_2H_4 purification.

Separation mechanism

To further understand the role of **CPOC-301** in the mechanism of selective C_2H_6/C_2H_4 adsorption, modelling studies based on first-principles dispersion-corrected density functional theory (DFT-D) calculations were performed. It was found that the primary adsorption sites for both C_2H_6 and C_2H_4 molecules are located at the calix[4]resorcinarene cavities. The lowest-energy gas binding configurations are shown in Figs. 4a and 4b. For clarity, only one adsorbed gas molecule at the calix[4]resorcinarene cavity site is shown, because the remaining five sites within **CPOC-301** are crystallographically identical. The corresponding calculated static binding energies (ΔE, $\Delta E = E_{POC+gas} - E_{POC} - E_{gas}$) of C_2H_6 and C_2H_4 are around − 63.4 and − 56.5 kJ mol^{-1}, respectively. Such binding energy variation suggests the stronger host-guest interactions between C_2H_6 and calix[4]resorcinarene cavity than that of C_2H_4, which is in accord with our aforementioned experimental observation. This can be ascribed to the more polarizable C_2H_6 in “matches” better to the electron-rich cavity of calix[4]resorcinarene than the less polarizable C_2H_4 molecule. As a result, the C − H···π interactions existing between the C_2H_6 and calix[4]resorcinarene cavity are stronger than those of the C_2H_4 molecule. To further authenticate our result, the host-guest interactions between **CPOC-301** and C_2H_2 (acetylene), another guest molecule of the C2 hydrocarbons family, has also been simulated (Fig. 4c). The calculated ΔE value of C_2H_2 is -51.7 kJ mol^{-1}, indicating that its host-guest interaction is weakest in the C2 hydrocarbons. This is consistent with the experimental Q_{st} results (20.2 kJ/mol for C_2H_2), and has been confirmed by C_2H_2/C_2H_4 breakthrough experiment (Fig. 5 and Supplementary Fig. 16).

Discussion

We have reported a pioneering work by using shape-persistent amine-linked **CPOC-301** as POC adsorbent for C_2H_4 purification for the first time. Specifically, the highly porous **CPOC-301** can efficiently trap C_2H_6 from C_2H_6/C_2H_4 mixture and therefore directly produce high-purity C_2H_4. The preferential interactions with C_2H_6 over C_2H_4 in **CPOC-301**, are due to the C_2H_6 form more multiple C−H···π hydrogen bonds with

resorcin[4]arene cavities than C_2H_4 guests as indicated by the results of DFT-D calculations. This finding may shed some light on the design and synthesis of POCs based on supramolecular cavitands as “porous additives” in column and membrane separation applications for industrially important gases in the future. Efforts to explore these possibilities are ongoing.

Method

Synthetic procedures of CPOC-301

All reagents and solvents are were purchased from Sinopharm Chemical Reagent Co., Ltd with analytical grade, and utilized as supplied without further purification. **CPOC-301** was synthesized according to the previously published procedure[56]. Typical synthesis processes were as follows: 162 mg (0.20 mmol) RC4ACHO[57] and 43 mg (0.4 mmol) *p*-phenylenediamine were added into 5 mL of nitrobenzene and 15 mL of $CHCl_3$. The mixture was sealed in a 48 mL pressure vial, and heated to 65 ° C with stirring for 2 days, and afterward cooled down naturally. Red block single crystals of **CPOC-301** with ~78% yield were obtained by the slow vapor diffusion of methanol into the abovementioned mixture.

Characterization of CPOC-301

The as-prepared **CPOC-301** sample was characterized by the following available instruments in Fujian Institute of Research on the Structure of Matter, Chinese Academy of Sciences, Fuzhou, Fujian, China. Proton nuclear magnetic resonance (1H NMR) data were recorded at ambient temperature a Burker AVANCE 400 (400 MHz) for spectrometer. Fourier-transformed infrared spectroscopy (FT-IR) spectra were taken on a Magna 750 FT-IR spectrometer using KBr pellets in the 600–4000 cm^{-1} region. High-resolution electrospray ionization mass spectrometry (ESI-TOF-MS) was recorded on a MaXis™ 4G instrument from Bruker. Thermal gravimetric analysis (TGA) was collected at a ramp rate of 10°C/min in dynamic nitrogen (N_2) flow within a temperature range of 30-900 °C with a NETZSCH STA 449C thermal analyzer. Powder X-ray diffraction (PXRD) pattern was performed on a Rigaku Mini 600 X-ray diffractometer for CuK_α radiation (λ = 0.154 Å), with a scan speed of 0.5°/min and a step size of 0.02° in 2θ.

Gas adsorption measurements

All the gas adsorption-desorption measurements of **CPOC-301** were carried out by using automatic volumetric adsorption equipment (Micromeritics, ASAP2020). Pore size distribution (PSD) data was obtained from the N_2 sorption isotherm at 77 K based on the DFT model in the Micromeritics ASAP 2020 software package (assuming cylinder pore geometry). Prior to the measurements, the samples were degassed at 100 ^{o}C under dynamic vacuum (below 10 μmHg) for 10 h to remove the adsorbed impurities. The calculated pore volume and the micropore volume are based on the ASAP 2020 physisorption analyzer's built-in software. The isosteric heat of sorption for C_2H_6 and C_2H_4 was calculated as a function of the gas uptake by comparing the adsorption isotherms at 273, 283 and 293 K. The data were modeled with a virial-type expression composed of parameters a_i and b_i (Equation 1), and the heat of adsorption (Q_{st}) was then calculated from the fitting parameters using Equation 2, where P is the pressure, N is the amount adsorbed, T is the temperature, R is the universal gas constant, and m and n determine the number of terms required to describe the isotherm adequately. The parameters were obtained from the fitting of the C_2H_6 and C_2H_4 adsorption isotherms. All isotherms were fitted with R^2>0.999. In order to evaluate the separation performance for C_2H_6/C_2H_4, we used the Ideal Adsorbed Solution Theory (IAST) of Myers and Prausnitz[58] along with the pure component isotherm fits by dual-site Langmuir-Freundlich equation to determine the molar loadings in the mixture for specified partial pressures in the bulk gas phase (Equation 3). Where N is molar loading of species (mmol g^{-1}), A is saturation capacity of species (mmol g^{-1}), B is Langmuir constant (kPa^{-c}), C is Freundlich constant and P is bulk gas phase pressure of species (kPa). The adsorption selectivity based on IAST for mixed C_2H_6/C_2H_4 is defined by the following equation 4.

$$ln_p = \ln N + \frac{1}{T}\sum_{i=0}^{m} a_i N^i + \sum_{i=0}^{n} b_i N^i \qquad \textbf{(Equation 1)}$$

$$Q_{st} = -R\sum_{i=0}^{m} a_i N^i \qquad \textbf{(Equation 2)}$$

$$N = A_1\frac{B_1 \times P^{C_1}}{1+B_1 \times P^{C_1}} + A_2\frac{B_2 \times P^{C_2}}{1+B_2 \times P^{C_2}} \qquad \textbf{(Equation 3)}$$

$$S_{A/B} = \frac{x_A y_B}{x_B y_A} \qquad \textbf{(Equation 4)}$$

Column Breakthrough Experiments

The mixed-gas breakthrough separation experiment was carried out using a home-built setup coupled with a mass spectrometer (Pfeiffer GSD320). For instance, in a typical breakthrough experiment for C_2H_4/C_2H_6/He (10:10:80, v/v/v) and C_2H_2/C_2H_4/He (10:10:80, v/v/v) gas mixtures, **CPOC-301** powder (0.39 g) was packed into a custom-made stainless-steel column (3.0 mm I.D.×120 mm) with silica wool filling the void space. The packed column was heated at 100 ^oC for 12 h under a constant He flow (10 mL min^{-1} at 298 K and 1 bar) to activate the sample. The flow of He was then turned off and a gas mixture of C_2H_4/C_2H_6/He (2 mL min^{-1}) was allowed to flow into the column. Outlet effluent from the column was continuously monitored using mass spectrometer. After the breakthrough experiment, the sample was regenerated in-situ in the column at 100 ^oC for 12 h. The complete breakthrough of C_2H_6 was indicated by the downstream gas composition reaching that of the feed gas. On the basis of the mass balance, the gas adsorption capacities can be determined as follows[59]:

$$q_i = \frac{C_i V}{22.4 \times m} \times \int_0^t \left(1 - \frac{F}{F_0}\right) dt$$

Where qi is the equilibrium adsorption capacity of gas i (mmol g^{-1}), C_i is the feed gas concentration, V is the volumetric feed flow rate (cm^3 min^{-1}), t is the adsorption time (min), F_0 and F are the inlet and outlet gas molar flow rates, respectively, and m is the mass of the adsorbent (g). The separation factor (α) of the breakthrough experiment is determined as:

$$\alpha = \frac{q_A y_B}{q_B y_A}$$

in which y_i is the molar fraction of gas i (i=A, B) in the gas mixture.

Binding energy calculations

The initial binding sites for C_2H_6, C_2H_4 and C_2H_2 were determined from simulated annealing calculations using Adsorption Locator Module in the Material Studio program package. The possible main adsorption sites for adsorbed C2 hydrocarbon molecules in **CPOC-301** were investigated by the $Dmol^3$ module in the

Material Studio program package. The PBE-type exchange-correlation functional with a generalized gradient approximation and the Double Numerical plus polarization (DNP) basis sets that include a d-type polarization function on all non-hydrogen atoms and a p-type polarization function on all hydrogen atoms were employed for all calculations. The FINE quality mesh size was employed in the calculations. During the C2-Cage structure optimization, the atomic positions of the **CPOC-301** were kept immobile and the single C2 hydrocarbon molecule was allowed to move during optimization. The adsorption energies were calculated in terms of equation:

$$\Delta E = E_{POC+gas} - E_{POC} - E_{gas}$$

where $E_{POC+gas}$ stands for the energy of the optimized adsorbate-Cage structure, and E_{POC}, and E_{gas} denote the energies of the bare Cage structure and the isolated C2 hydrocarbon molecule, respectively. According to this equation, more negative adsorption energy means more favorable binding.

References

1. Matar S. & Hatch L. F. Chemistry of petrochemical processes. *Gulf Professional Publishing*. (2001).
2. Ren T., Patel M. & Blok K. Olefins from conventional and heavy feedstocks: Energy use in steam cracking and alternative pocesses. *Energy.* **31**, 425–451 (2006).
3. Zhao X., Wang Y., Li D.-S., Bu X. & Feng P. Metal-organic frameworks for separation. *Adv. Mater.* **30**, 1705189 (2018).
4. Bao Z., Chang G., Xing H., Krishna R., Ren Q. & Chen B. Potential of microporous metal–organic frameworks for separation of hydrocarbon mixtures. *Energy Environ. Sci.* **9**, 3612–3641 (2016).
5. Qazvini O. T., Babarao R., Shi Z.-L., Zhang Y.-B. & Telfer S. G. A robust ethane-trapping metal-organic framework with a high capacity for ethylene purification. *J. Am. Chem. Soc.* **141**, 5014–5020 (2019).
6. Li L., *et al.* Ethane/ethylene separation in a metal-organic framework with iron-peroxo sites. *Science.* **362**, 443–446 (2018).
7. Hao H. G., *et al.* Simultaneous trapping of C_2H_2 and C_2H_6 from a ternary mixture of $C_2H_2/C_2H_4/C_2H_6$ in a robust metal-organic framework for the purification of C_2H_4. *Angew. Chem. Int. Ed.* **57**, 16067–16071 (2018).
8. Lin R. B., *et al.* Boosting ethane/ethylene separation within isoreticular ultramicroporous metal-organic frameworks. *J. Am. Chem. Soc.* **140**, 12940–12946 (2018).
9. Zeng H., *et al.* Cage-interconnected metal-organic framework with tailored apertures for efficient C_2H_6/C_2H_4 separation under humid conditions. *J. Am. Chem. Soc.* **141**, 20390–20396 (2019).

10. Liao P.-Q., Zhang W. X., Zhang J. P. & Chen X. M. Efficient purification of ethene by an ethane-trapping metal-organic framework. *Nat. Commun.* **6**, 9697 (2015).
11. Pei J., *et al.* Engineering microporous ethane-trapping metal–organic frameworks for boosting ethane/ethylene separation. *J. Mater. Chem. A.* **8**, 3613–3620 (2020).
12. Segura J. L., Mancheno M. J. & Zamora F. Covalent organic frameworks based on schiff-base chemistry: Synthesis, properties and potential applications. *Chem. Soc. Rev.* **45**, 5635–5671 (2016).
13. Wang Z., Zhang S., Chen Y., Zhang Z. & Ma S. Covalent organic frameworks for separation applications. *Chem. Soc. Rev.* **49**, 708–735 (2020).
14. Zhang X., *et al.* Selective ethane/ethylene separation in a robust microporous hydrogen-bonded organic framework. *J. Am. Chem. Soc.* **142**, 633–640 (2020).
15. Mastalerz M. Porous shape-persistent organic cage compounds of different size, geometry, and function. *Acc. Chem. Res.* **51**, 2411–2422 (2018).
16. Zhang G. & Mastalerz M. Organic cage compounds - from shape-persistency to function. *Chem. Soc. Rev.* **43**, 1934–1947 (2014).
17. Hasell T. & Cooper A. I. Porous organic cages: Soluble, modular and molecular pores. *Nat. Rev. Mater.* **1**, 16053 (2016).
18. Liu T. & Liu G. Porous organic materials offer vast future opportunities. *Nat. Commun.* **11**, 4984 (2020).
19. Thomas A. Much ado about nothing – a decade of porous materials research. *Nat. Commun.* **11**, 4985 (2020).
20. Acharyya K. & Mukherjee P. S. Organic imine cages: Molecular marriage and applications. *Angew. Chem. Int. Ed.* **58**, 8640–8653 (2019).
21. Song Q., *et al.* Porous organic cage thin films and molecular-sieving membranes. *Adv. Mater.* **28**, 2629–2637 (2016).
22. Bushell A. F., *et al.* Nanoporous organic polymer/cage composite membranes. *Angew. Chem. Int. Ed.* **52**, 1253–1256 (2013).
23. Yuan Y. D., *et al.* Porous organic cages as synthetic water channels. *Nat. Commun.* **11**, 4927 (2020).
24. Tozawa T., *et al.* Porous organic cages. *Nat. Mater.* **8**, 973–978 (2009).
25. Jin Y., Voss B. A., Jin A., Long H., Noble R. D. & Zhang W. Highly co_2-selective organic molecular cages: What determines the co_2 selectivity. *J. Am. Chem. Soc.* **133**, 6650–6658 (2011).
26. Liu C., *et al.* Elucidating heterogeneous photocatalytic superiority of microporous porphyrin organic cage. *Nat. Commun.* **11**, 1047 (2020).
27. Greenaway R., *et al.* High-throughput discovery of organic cages and catenanes using computational screening fused with robotic synthesis. *Nat. Commun.* **9**, 2849 (2018).
28. Liu M., *et al.* Three-dimensional protonic conductivity in porous organic cage solids. *Nat. Commun.* **7**, 12750 (2016).

29. Hong S., *et al.* Porphyrin boxes: Rationally designed porous organic cages. *Angew. Chem. Int. Ed.* **54**, 13241–13244 (2015).
30. Avellaneda A., *et al.* Kinetically controlled porosity in a robust organic cage material. *Angew. Chem. Int. Ed.* **52**, 3746–3749 (2013).
31. Zhang G., Presly O., White F., Oppel I. M. & Mastalerz M. A shape-persistent quadruply interlocked giant cage catenane with two distinct pores in the solid state. *Angew. Chem. Int. Ed.* **53**, 5126–5130 (2014).
32. Mastalerz M., Schneider M. W., Oppel I. M. & Presly O. A salicylbisimine cage compound with high surface area and selective co_2/ch_4 adsorption. *Angew. Chem. Int. Ed.* **50**, 1046–1051 (2011).
33. Little M. A., *et al.* Trapping virtual pores by crystal retro-engineering. *Nat. Chem.* **7**, 153–159 (2015).
34. Slater A. G., *et al.* Reticular synthesis of porous molecular 1d nanotubes and 3d networks. *Nat. Chem.* **9**, 17–25 (2017).
35. Sun N., *et al.* Multifunctional tubular organic cage-supported ultrafine palladium nanoparticles for sequential catalysis. *Angew. Chem. Int. Ed.* **58**, 18011–18016 (2019).
36. Zhang G., Presly O., White F., Oppel I. M. & Mastalerz M. A permanent mesoporous organic cage with an exceptionally high surface area. *Angew. Chem. Int. Ed.* **53**, 1516–1520 (2014).
37. Schneider M. W., *et al.* Periphery-substituted [4 + 6] salicylbisimine cage compounds with exceptionally high surface areas: Influence of the molecular structure on nitrogen sorption properties. *Chem. Eur. J.* **18**, 836–847 (2012).
38. Chen L., *et al.* Separation of rare gases and chiral molecules by selective binding in porous organic cages. *Nat. Mater.* **13**, 954–960 (2014).
39. Hasell T., *et al.* Porous organic cages for sulfur hexafluoride separation. *J. Am. Chem. Soc.* **138**, 1653–1659 (2016).
40. Liu M., *et al.* Barely porous organic cages for hydrogen isotope separation. *Science.* **366**, 613–620 (2019).
41. Wang Z., *et al.* Soft porous crystal based upon organic cages that exhibit guest-induced breathing and selective gas separation. *J. Am. Chem. Soc.* **141**, 9408–9414 (2019).
42. Timmerman P., Verboom W. & Reinhoudt D. N. Resorcinarenes. *Tetrahedron.* **52**, 2663–2704 (1996).
43. MacGillivray L. R. & Atwood J. L. A chiral spherical molecular assembly held together by 60 hydrogen bonds. *Nature.* **389**, 469–472 (1997).
44. Avram L., Cohen Y. & Rebek J., Jr. Recent advances in hydrogen-bonded hexameric encapsulation complexes. *Chem. Commun.* **47**, 5368–5375 (2011).
45. Kane C. M., Ugono O., Barbour L. J. & Holman K. T. Many simple molecular cavitands are intrinsically porous (zero-dimensional pore) materials. *Chem. Mater.* **27**, 7337–7354 (2015).
46. Gropp C., Quigley B. L. & Diederich F. Molecular recognition with resorcin[4]arene cavitands: Switching, halogen-bonded capsules, and enantioselective complexation. *J. Am. Chem. Soc.* **140**, 2705–2717 (2018).

47. Kane C. M., Banisafar A., Dougherty T. P., Barbour L. J. & Holman K. T. Enclathration and confinement of small gases by the intrinsically 0d porous molecular solid, Me,H,SiMe$_2$. *J. Am. Chem. Soc.* **138**, 4377–4392 (2016).
48. Cavarzan A., Scarso A., Sgarbossa P., Strukul G. & Reek J. N. H. Supramolecular control on chemo- and regioselectivity via encapsulation of (nhc)-au catalyst within a hexameric self-assembled host. *J. Am. Chem. Soc.* **133**, 2848–2851 (2011).
49. Kobayashi K. & Yamanaka M. Self-assembled capsules based on tetrafunctionalized calix[4]resorcinarene cavitands. *Chem. Soc. Rev.* **44**, 449–466 (2015).
50. Skala L. P., Yang A., Klemes M. J., Xiao L. & Dichtel W. R. Resorcinarene cavitand polymers for the remediation of halomethanes and 1,4-dioxane. *J. Am. Chem. Soc.* **141**, 13315–13319 (2019).
51. Barrett E. S., Irwin J. L., Edwards A. J. & Sheburn M. S. Superbowl container molecules. *J. Am. Chem. Soc.* **126**, 16747–16749 (2004).
52. Wierzbicki M., Glowacka A. A., Szymanski M. P. & Szumna A. A chiral member of the family of organic hexameric cages. *Chem. Commun.* **53**, 5200–5203 (2017).
53. Su K., Wu M., Yuan D. & Hong M. Interconvertible vanadium-seamed hexameric pyrogallol 4 arene nanocapsules. *Nat. Commun.* **9**, 4941 (2018).
54. Sun J., Bennett J. L., Emge T. J. & Warmuth R. Thermodynamically controlled synthesis of a chiral tetra-cavitand nanocapsule and mechanism of enantiomerization. *J. Am. Chem. Soc.* **133**, 3268–3271 (2011).
55. Su K., Wang W., Li B. & Yuan D. Azo-bridged calix 4 resorcinarene-based porous organic frameworks with highly efficient enrichment of volatile iodine. *ACS Sustainable Chem. Eng.* **6**, 17402–17409 (2018).
56. Su K., Wang W., Du S., Ji C., Zhou M. & Yuan D. Reticular chemistry in the construction of porous organic cages. *J. Am. Chem. Soc.*, 18060–18072 (2020).
57. Grajda M., Wierzbicki M., Cmoch P. & Szumna A. Inherently chiral iminoresorcinarenes through regioselective unidirectional tautomerization. *J. Org. Chem.* **78**, 11597–11601 (2013).
58. Myers A. L. & Prausnitz J. M. Thermodynamics of mixed-gas adsorption. *AIChE J.* **11**, 121–122 (1965).
59. Liu J., Tian J., Thallapally P. K. & McGrail B. P. Selective CO_2 capture from flue gas using metal-organic frameworks-a fixed bed study. *J. Phys. Chem. C.* **116**, 9575–9581 (2012).

Declarations

Conflict of interest

The authors state that they have no conflict of interest.

Acknowledgments

This work was financially supported by the National Key R&D Program of China (2017YFA0700102), the National Natural Science Foundation of China (22071244, 21707143), and the Strategic Priority Research Program of the Chinese Academy of Sciences (XDB20000000).

Author contributions

Daqiang Yuan and Kongzhao Su proposed the ideas and supervised the project. Kongzhao Su, and Shunfu Du prepared the cages and carried out the characterization of the cages. Wenjing Wang and Chunqing Ji performed the gas sorption and separation experiments. Daqiang Yuan, Kongzhao Su and Wenjing Wang analyzed the data and wrote the manuscript. All authors discussed the results and commented on the manuscript.

Additional information

Supplementary Information accompanies this paper at http://www.nature.com/naturecommunications.

Competing financial interests

The authors declare no competing financial interests.

Figures

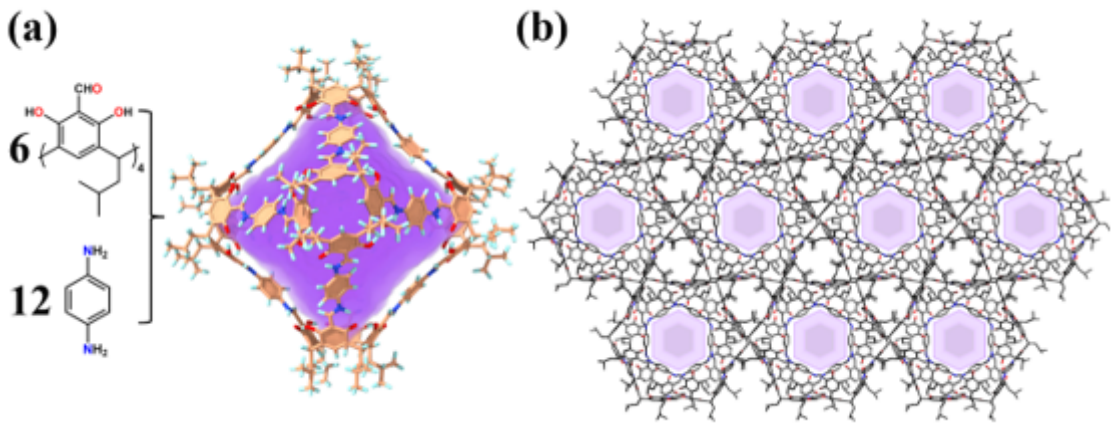

Figure 1

Schematic illustration for assembly of CPOC-301. a The X-ray crystal structure of CPOC-301. b Molecular packing of CPOC-301 in solid state viewed from [001] direction; hydrogen atoms are omitted for clarity.

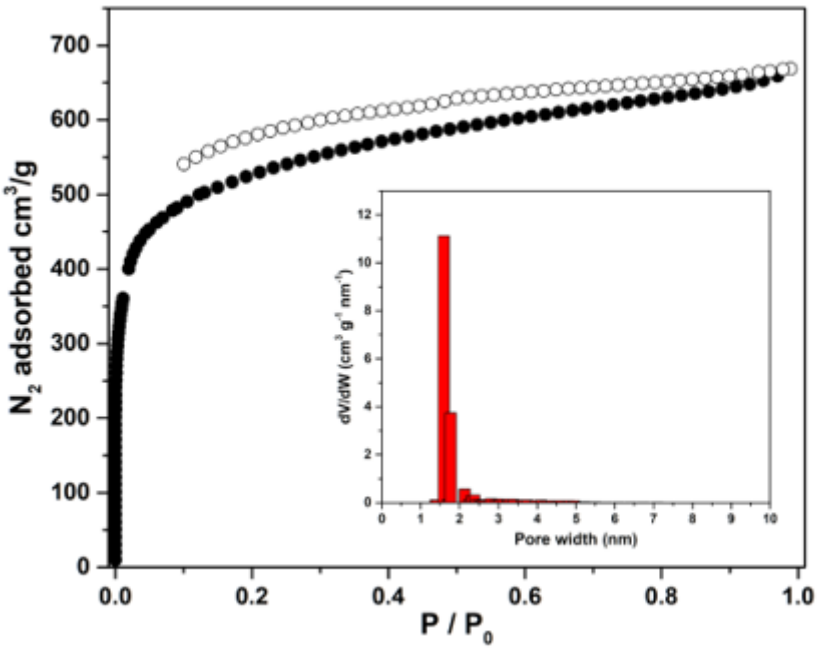

Figure 2

Porosity measurements. N2 gas sorption isotherm at 77 K for CPOC-1, inset: BET plot for surface area calculation, and the inset shows the calculated PSD of CPOC-1.

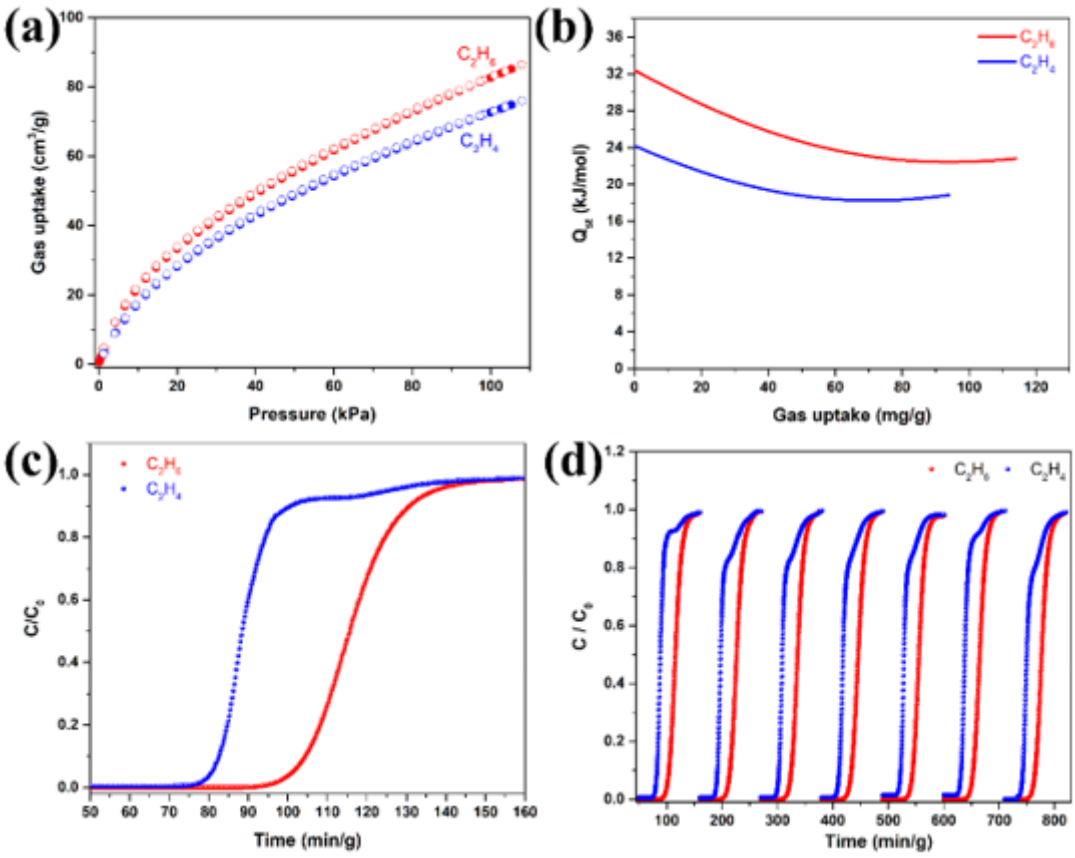

Figure 3

C2H4/C2H6 separation performances. a Experimental C2H6 and C2H4 adsorption isotherms of CPOC-301 at 293 K. b Isosteric heat of adsorption plots for the adsorption by CPOC-301. c Experimental breakthrough curves for an equimolar C2H4/C2H6 mixture at 298 K and 1 bar over a packed bed of CPOC-301. d The recyclability of CPOC-301 under multiple mixed-gas column breakthrough tests.

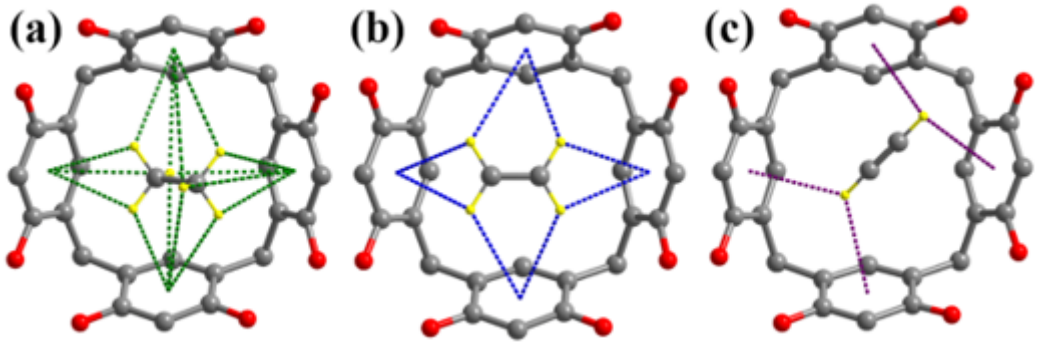

Figure 4

Mechanism study. Comparison of the preferential a C2H6, b C2H4 and c C2H2 adsorption sites and the close C–H···π interactions within the cavities of calix[4]resorcinarene observed by DFT-D calculations. Carbon is grey, oxygen red and hydrogen yellow. Dashed bonds highlight C–H···π interactions.

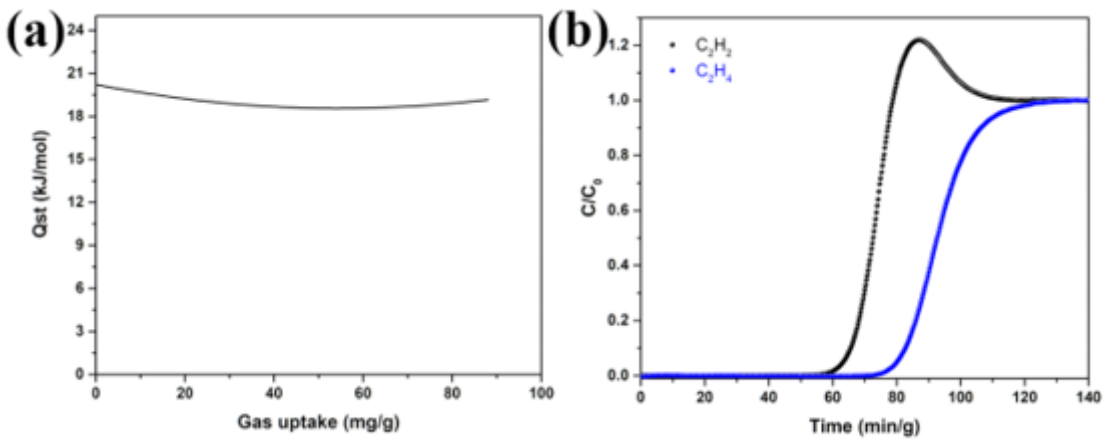

Figure 5

C2H4/C2H2 separation performances. a Isosteric heat of adsorption plots for the adsorption of C2H2 by CPOC-301. b The experimental column breakthrough curve of CPOC-301 with an equimolar C2H2/C2H4 mixture.

Supplementary Files

This is a list of supplementary files associated with this preprint. Click to download.

- NCESI.docx
- sipdfcanon.pdf